2007 IEEE International Conference on
Robotics and Automation
Roma, Italy, 10-14 April 2007

Dynamic Analyses of Underactuated Virtual Passive Dynamic Walking

Fumihiko Asano and Zhi-Wei Luo

Abstract— **Realization of an energy-efficient and high-speed dynamic walking has come to be one of the main subjects in the research area of robotic biped locomotion, and passive dynamic walking has been widely attracted as a clue to solve the problem. It has been empirically known that the effect of convex curve shape of foot, which characterizes passive-dynamic walkers, is important to increase walking speed. This paper then investigates the driving mechanism of compass-like biped robots and the rolling effect of semicircular feet are mainly investigated. We first analyze the mechanism of a planar fully-actuated compass-like biped model to clarify the importance of ankle-joint torque introducing generalized virtual gravity concept. In the second, a planar underactuated biped model with semicircular feet is introduced and we show that virtual passive dynamic walking by hip-joint torque only can be realized based on the rolling effect. We then compare with a flat feet model through linear approximation, and show that the rolling effect is equivalent to its virtual ankle-joint torque. Throughout this paper, we provide novel insights into how ZMP-free robots can generate a dynamic bipedal gait.**

I. Introduction

Passive dynamic walking (PDW) [2] has been considered as a clue to elucidate the mechanism of energy-efficient dynamic walking. By imitating or modifying the PDW mechanism, several energy-efficient dynamic bipedal walking robots have been realized so far [7][3][4][5][9]. Major PDW-inspired approaches to biped robot control tend to actuate a simple legged machine gently by small power motors, and are surely successful ways to achieve an efficient biped locomotion. On the other hand, convex curve shape of the feet also characterizes passive dynamic walkers [2], and is not a feature of recent biped humanoid robots controlled based on zero moment point (ZMP) [1]. The importance of such foot shape or the rolling effect has been empirically recognized [8][5], however, until now its theoretical investigation has not been done.

Based on the observation, this paper studies the rolling effect of semicircular feet on dynamic bipedal walking through theoretical investigation and numerical analysis. We consider the mechanism from the view point of generalized virtual gravity concept [5] and clarify how the rolling effect accelerates the robot's center of mass (CoM) during stance phase.

In this paper, we first introduce a fully-actuated compass-like biped robot with flat feet and analyze the relation between the CoM and the joint torques based on the inverse transformation and generalized virtual gravity concept. The importance of the ankle-joint torque is clarified. Secondly, an underactuated compass-like biped robot with semicircular feet and underactuated virtual passive dynamic walking by hip-joint torque only are introduced. It is then clarified that the dynamics of semicircular feet model can be transformed to that of a fully-actuated model with flat feet and the rolling effect functions as the ankle-joint torque through linearization of the two walking systems and their comparisons. It is theoretically shown that the rolling effect accelerates the robot's CoM forward as a virtual ankle-joint torque together with the real hip-joint one during stance phase. Throughout this paper, the authors provide novel insights for biped walking control as *ZMP-free robots*.

F. Asano and Z.W. Luo are with Bio-Mimetic Control Research Center, RIKEN, Nagoya 463-0003, Japan asano@bmc.riken.jp

Z.W. Luo is with the Dept. of Computer and Systems Engineering, Faculty of Engineering, Kobe University, Kobe 657-8501, Japan luo@gold.kobe-u.ac.jp

II. Model and Mechanism of Planar Fully-actuated Compass-like Biped Robot

This paper first considers a planar fully-actuated compass-like biped robot as shown in Fig. 1. The details of biped model is described and the relation between the CoM and the joint torques is investigated.

A. Mathematical model

This subsection describes the mathematical model of a planar fully-actuated compass-like biped robot shown in Fig. 1, which consists of two leg links and three point masses and has flat feet whose mass and thin can be neglected. The dynamic equation is given by

$$\boldsymbol{M}(\boldsymbol{\theta})\ddot{\boldsymbol{\theta}} + \boldsymbol{C}(\boldsymbol{\theta},\dot{\boldsymbol{\theta}})\dot{\boldsymbol{\theta}} + \boldsymbol{g}(\boldsymbol{\theta}) = \boldsymbol{S}\boldsymbol{u} = \begin{bmatrix} 1 & 1 \\ 0 & -1 \end{bmatrix} \begin{bmatrix} u_1 \\ u_2 \end{bmatrix} \quad (1)$$

where $\boldsymbol{\theta} = \begin{bmatrix} \theta_1 & \theta_2 \end{bmatrix}^{\mathrm{T}}$ is the generalized coordinate vector, $\boldsymbol{S}\boldsymbol{u}$ is the control input; u_1 and u_2 are the ankle-joint torque and the hip-joint one, respectively. We assume that the stance foot is always in contact with the ground at exactly one point without slipping and has enough length according to the ZMP range.

Total mechanical energy of the robot, E [J], is determined as the sum of kinetic and potential energy and given by

$$E(\boldsymbol{\theta},\dot{\boldsymbol{\theta}}) = \frac{1}{2}\dot{\boldsymbol{\theta}}^{\mathrm{T}}\boldsymbol{M}(\boldsymbol{\theta})\dot{\boldsymbol{\theta}} + P(\boldsymbol{\theta}). \quad (2)$$

Its time derivative satisfies the following relation

$$\dot{E} = \dot{\boldsymbol{\theta}}^{\mathrm{T}}\boldsymbol{S}\boldsymbol{u}. \quad (3)$$

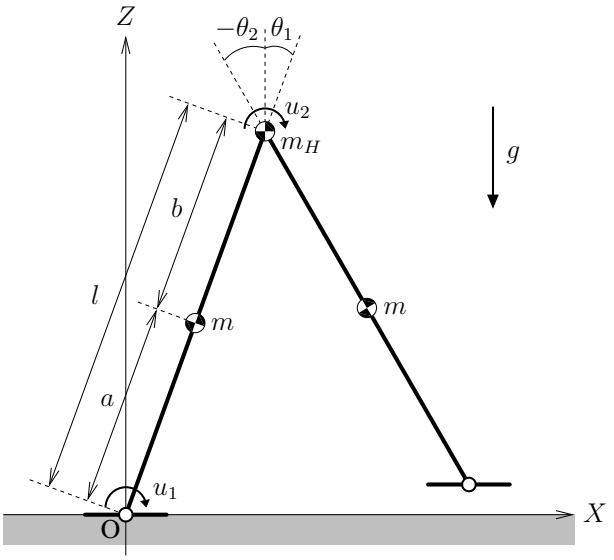

Fig. 1. Model of planar fully-actuated compass-like biped robot with flat feet

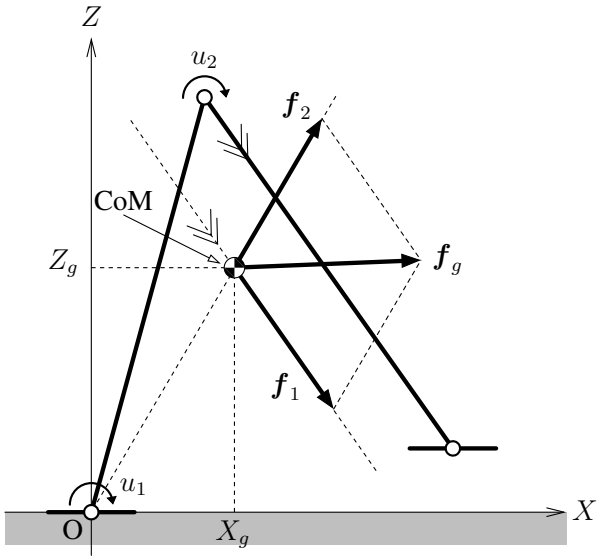

Fig. 2. Relations between generalized virtual gravity vectors at CoM and joint torques

B. Relation between center of mass and joint torques

Let $\boldsymbol{r}_g = \begin{bmatrix} X_g & Z_g \end{bmatrix}^{\mathrm{T}}$ be the positional vector of CoM, and its time derivative yields $\dot{\boldsymbol{r}}_g = \boldsymbol{J}_g(\boldsymbol{\theta})\dot{\boldsymbol{\theta}}$ where $\boldsymbol{J}_g(\boldsymbol{\theta}) \in R^{2\times 2}$ is the corresponding Jacobian matrix, which has a singularity at $\theta_1 = \theta_2$. Except this condition, the following inverse transformation from the joint torques to the translation force at the CoM is possible.

$$\boldsymbol{f}_g = \boldsymbol{J}_g(\boldsymbol{\theta})^{-\mathrm{T}}\boldsymbol{S}\boldsymbol{u} \tag{4}$$

We call the translation force, $\boldsymbol{f}_g \in R^2$, *generalized virtual gravity*, which represents a 2-dimensional driving force exerting at the robot's CoM. Eq. (4) can be rearranged as

$$\begin{aligned} \boldsymbol{f}_g &= \boldsymbol{J}_g(\boldsymbol{\theta})^{-\mathrm{T}} \left(\begin{bmatrix} 1 \\ 0 \end{bmatrix} u_1 + \begin{bmatrix} 1 \\ -1 \end{bmatrix} u_2 \right) \\ &= \frac{mbu_1}{M\Delta_g} \begin{bmatrix} \sin\theta_2 \\ \cos\theta_2 \end{bmatrix} - \frac{r_g u_2}{\Delta_g} \frac{\boldsymbol{r}_g}{r_g} \\ &=: \boldsymbol{f}_1 + \boldsymbol{f}_2 \end{aligned} \tag{5}$$

where $r_g := |\boldsymbol{r}_g|$, $M := m_H + 2m$ is the robot's total mass and

$$\Delta_g := \det(\boldsymbol{J}_g) = -\frac{mb(m_H l + ma + ml)\sin(\theta_1 - \theta_2)}{M^2}. \tag{6}$$

Note that Eq. (5) is written in the form consisting of two unit vectors. Eq. (5) shows that the effect of ankle-joint torque, $\boldsymbol{f}_1$, yields being parallel to the swing leg and that of the hip-joint torque, $\boldsymbol{f}_2$, yields central force as shown in Fig. 2. Since $\boldsymbol{f}_g$ has a singularity at $\theta_1 = \theta_2$, both vectors $\boldsymbol{f}_1$ and $\boldsymbol{f}_2$ diverges at this point and it is unsuitable to examine the torque distribution effect based on this approach. The ratio of $|\boldsymbol{f}_1|$ to $|\boldsymbol{f}_2|$ is, however, kept finite regardless of the singularity so long as u_2 is not zero, which yields

$$\frac{|\boldsymbol{f}_1|}{|\boldsymbol{f}_2|} = \frac{mbu_1}{Mr_g u_2}. \tag{7}$$

In order to realize $|\boldsymbol{f}_1| = |\boldsymbol{f}_2|$, as described in [5], magnitude of u_2 is much more required than that of u_1. In other words, u_2 is more sensitive to $\boldsymbol{f}_g$ than u_1 in the meaning of vector norm. In this sense u_2 seems to be more advantageous than u_1 to propel the CoM forward, however, excessive use of u_2 or small μ yields increasing the gravity during the first half of cycle (See Figs. 6 and 10) and disturbing to overcome the potential barrier at midstance.

In the next section, we propose an approach based on orthogonal projection of $\boldsymbol{f}_i$ on $\dot{\boldsymbol{r}}_g$ to avoid the singularity.

III. Analysis of Virtual Passive Dynamic Walking

It is known that the ankle-joint torque is relatively important and effective to drive the robot's CoM forward. This section investigates the mechanism of the joint torques' effect and clarifies the importance of the ankle-joint torque from the generalized virtual gravity point of view.

A. Virtual passive dynamic walking

Let i be the link number $(1, 2, \cdots)$ or the hip position (H) in the following, and their corresponding X-positions at each link's CoM are denoted as X_i. Time derivative of X_i is further denoted as $\dot{X}_i = \boldsymbol{J}_{X_i}\dot{\boldsymbol{\theta}}$ where $\boldsymbol{J}_{X_i} \in R^{1\times 2}$ is the Jacobian matrix corresponding to X_i. If we suppose a uniform virtual gravity whose magnitude is $g\tan\phi$ in X-direction, where ϕ [rad] represents the virtual slope angle [3], its equivalent transformed torque of the total virtual gravity effect $\boldsymbol{S}\boldsymbol{u}_{\mathrm{vg}}$ can be expressed as

$$\boldsymbol{S}\boldsymbol{u}_{\mathrm{vg}} = \sum_i m_i g \tan\phi \boldsymbol{J}_{X_i}(\boldsymbol{\theta})^{\mathrm{T}}, \tag{8}$$

TABLE I
PHYSICAL PARAMETERS OF THE ROBOT

m_H	10.0	kg
m	5.0	kg
$l\ (=a+b)$	1.0	m
a	0.5	m
b	0.5	m

and time derivative of E is then derived as follows.

$$\begin{aligned}\dot{E} &= \dot{\boldsymbol{\theta}}^{\mathrm{T}}\boldsymbol{S}\boldsymbol{u}_{\mathrm{vg}} = g\tan\phi\sum_i m_i\dot{\boldsymbol{\theta}}^{\mathrm{T}}\boldsymbol{J}_{X_i}(\boldsymbol{\theta})^{\mathrm{T}} \\ &= g\tan\phi\sum_i m_i\dot{X}_i = Mg\tan\phi\frac{\mathrm{d}}{\mathrm{d}t}\sum_i\frac{m_iX_i}{M} \\ &= Mg\tan\phi\dot{X}_g \end{aligned} \tag{9}$$

This leads the following relation:

$$\frac{\partial E}{\partial X_g} = Mg\tan\phi, \tag{10}$$

which is the unified property of passive dynamic walking. Following Eqs. (3) and (9), we obtain

$$\dot{E} = \dot{\boldsymbol{\theta}}^{\mathrm{T}}\boldsymbol{S}\boldsymbol{u} = Mg\tan\phi\dot{X}_g, \tag{11}$$

which specifies the relation between the robot's total mechanical energy and the X-position of CoM. Since this equation has a redundancy of the control inputs, we have to introduce another constraint condition. Let us then consider a solution by constant torque ratio, μ, which gives the condition of $u_1 = \mu u_2$. By substituting this into Eq. (11), the solution $\boldsymbol{S}\boldsymbol{u}$ is determined as

$$\boldsymbol{S}\boldsymbol{u} = \begin{bmatrix}\mu+1\\-1\end{bmatrix}\frac{Mg\tan\phi\dot{X}_g}{(\mu+1)\dot{\theta}_1 - \dot{\theta}_2}. \tag{12}$$

We call this solution *CTR formula* [4]. Note that this solution no longer has the meaning of a uniform virtual gravity in the X-direction. The inverse transformation of this $\boldsymbol{S}\boldsymbol{u}$ should yield the generalized virtual gravity vector.

B. Typical behaviours of generalized virtual gravity

Fig. 3 shows the generalized virtual gravity vector along the CoM orbit in the case of VPDW where $\phi = 0.02$ [rad]; (a) $\mu = 2.5$, (b) $\mu = 8.0$. The robot's physical parameters are chosen as Table I. As seen from the results, the vectors are going to diverge as the system closes with the singular point of $\theta_1 = \theta_2$. As reported in [4], the walking system's performance in the case of $\mu = 8.0$ is better or the walking speed is faster than that in the case of $\mu = 2.5$. The results strongly appeal that the generalized virtual gravity in the case of $\mu = 8.0$ accelerates the CoM more effectively than that of $\mu = 2.5$, and this supports the Asano's result in [4]. As shown in Fig. 3, the generalized virtual gravity of $\mu = 2.5$ has the unnecessary element perpendicular to $\dot{\boldsymbol{r}}_g$ more than that of $\mu = 8.0$, and this force element disrupts the forward acceleration of CoM as described later.

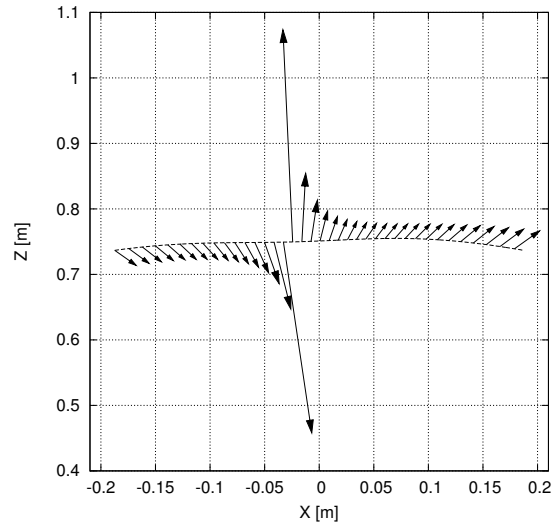

(a) $\mu = 2.5$

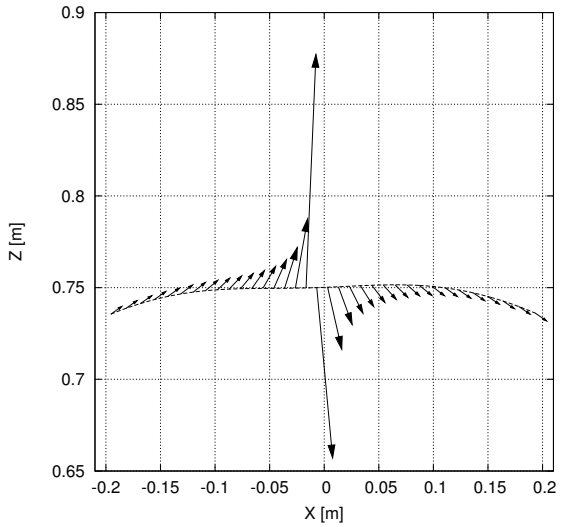

(b) $\mu = 8.0$

Fig. 3. Generalized virtual gravity vectors in virtual passive dynamic walking with CTR formula

C. Analysis based on orthogonal projection on $\dot{\boldsymbol{r}}_g$

The following relation is derived easily in the case of $\theta_1 \neq \theta_2$.

$$\dot{E} = \dot{\boldsymbol{\theta}}^{\mathrm{T}}\boldsymbol{S}\boldsymbol{u} = \dot{\boldsymbol{\theta}}^{\mathrm{T}}\boldsymbol{J}_g^{\mathrm{T}}\boldsymbol{J}_g^{-\mathrm{T}}\boldsymbol{S}\boldsymbol{u} = \dot{\boldsymbol{r}}_g^{\mathrm{T}}\boldsymbol{f}_g \tag{13}$$

Hence Eq. (11) can be interpreted the special case of Eq. (13) with the generalized virtual gravity vector in the form

$$\boldsymbol{f}_g = \begin{bmatrix}Mg\tan\phi\\0\end{bmatrix}. \tag{14}$$

In other words, Eq. (13) is the 2-dimensional case or the generalized case of Eq. (11). Let ${}^p\boldsymbol{f}_g$ be the orthogonal projection vector of $\boldsymbol{f}_g$ on $\dot{\boldsymbol{r}}_g$, considering Eq. (13), it is given by

$${}^p\boldsymbol{f}_g = \frac{\dot{\boldsymbol{r}}_g^{\mathrm{T}}\boldsymbol{f}_g}{\dot{r}_g^2}\dot{\boldsymbol{r}}_g = \frac{\dot{E}}{\dot{r}_g^2}\dot{\boldsymbol{r}}_g \tag{15}$$

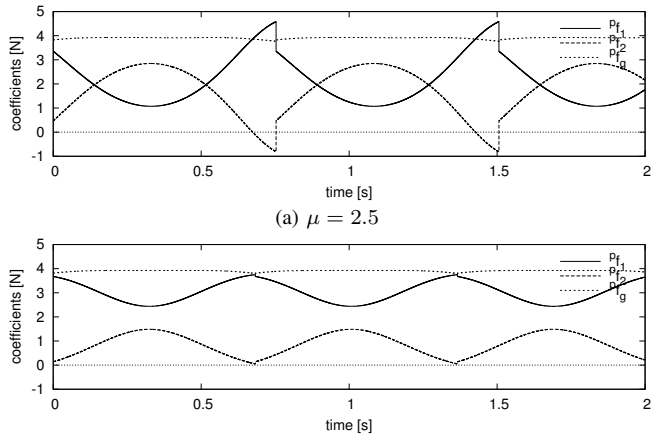

(a) $\mu = 2.5$

(b) $\mu = 8.0$

Fig. 4. Time evolutions of coefficients of orthogonal projective vectors ${}^{p}f_1$, ${}^{p}f_2$ and ${}^{p}f_g$

and this can be divided into two parts; $\boldsymbol{f}_1$ by the ankle-joint effect and $\boldsymbol{f}_2$ by the hip-joint effect, as follows.

$$\begin{aligned} {}^{p}\boldsymbol{f}_g &= \frac{\dot\theta_1 u_1 + \left(\dot\theta_1 - \dot\theta_2\right) u_2}{\dot r_g^2}\dot{\boldsymbol{r}}_g \\ &= \frac{\dot\theta_1 u_1}{\dot r_g}\frac{\dot{\boldsymbol{r}}_g}{\dot r_g} + \frac{\left(\dot\theta_1 - \dot\theta_2\right) u_2}{\dot r_g}\frac{\dot{\boldsymbol{r}}_g}{\dot r_g} \\ &=: {}^{p}\boldsymbol{f}_1 + {}^{p}\boldsymbol{f}_2 \end{aligned} \tag{16}$$

This projection enables to avoid the divergence at $\theta_1 = \theta_2$. We remark that the norm ratio yields the power ratio as follows.

$$\frac{|{}^{p}\boldsymbol{f}_1|}{|{}^{p}\boldsymbol{f}_2|} = \frac{\left|\dot\theta_1 u_1\right|}{\left|\left(\dot\theta_1 - \dot\theta_2\right) u_2\right|} \tag{17}$$

We further define the coefficients of ${}^{p}\boldsymbol{f}_1$, ${}^{p}\boldsymbol{f}_2$ and ${}^{p}\boldsymbol{f}_g$ respectively as follows.

$${}^{p}f_1 := \frac{\dot\theta_1 u_1}{\dot r_g}, \quad {}^{p}f_2 := \frac{\left(\dot\theta_1 - \dot\theta_2\right) u_2}{\dot r_g}, \quad {}^{p}f_g := \frac{\dot E}{\dot r_g} \tag{18}$$

Fig. 4 shows the time evolutions of ${}^{p}f_1$, ${}^{p}f_2$ and ${}^{p}f_g$ in VPDW with CTR formula where $\mu = 2.5$ and 8.0. In VPDW case, considering $\dot X_g > 0$, the following inequality holds.

$${}^{p}f_g = \frac{Mg\tan\phi\dot X_g}{\sqrt{\dot X_g^2 + \dot Z_g^2}} \le \frac{Mg\tan\phi\dot X_g}{\dot X_g} = Mg\tan\phi \tag{19}$$

If $\dot Z_g$ is 0 or sufficiently small, the equality in Eq. (19) holds. In general, ${}^{p}f_g \approx Mg\tan\phi$ regardless of the system's parameter choice because $\dot Z_g$ is small and is strongly supported by Fig. 4. We therefore conclude that, regardless of μ, the vector $\boldsymbol{f}_g$ has the magnitude of about $Mg\tan\phi$ in the $\dot{\boldsymbol{r}}_g$-direction, and the reason why the walking speed is decreased when μ is small cannot be explained by above investigation.

We now define the orthogonal vector of ${}^{p}f_g$ as follows:

$${}^{p}\boldsymbol{f}_g^{\perp} := \boldsymbol{f}_g - {}^{p}\boldsymbol{f}_g, \tag{20}$$

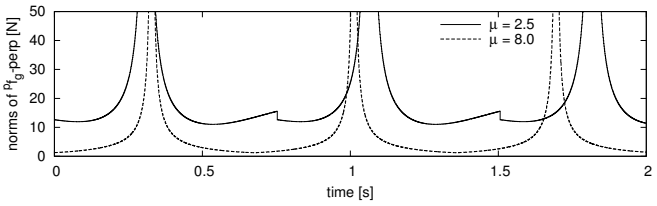

Fig. 5. Time evolution of norms of ${}^{p}\boldsymbol{f}_g^{\perp}$ for $\mu = 2.5$ and 8.0 in virtual passive dynamic walking with CTR formula

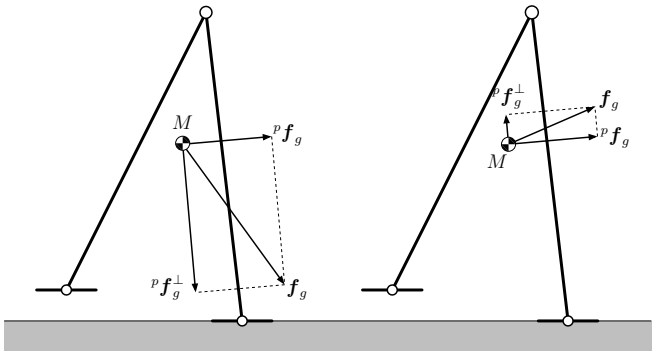

(a) μ is small (b) μ is large

Fig. 6. Generalized virtual gravity conditions for small and large μ

and compare this magnitude with that of ${}^{p}\boldsymbol{f}_g$. Note that ${}^{p}\boldsymbol{f}_g^{\perp}$ does not contribute the mechanical energy restoration, that is, $\dot{\boldsymbol{r}}_g^{\mathrm{T}}{}^{p}\boldsymbol{f}_g^{\perp} = 0$. Fig. 5 shows the time evolutions of $\left|{}^{p}\boldsymbol{f}_g^{\perp}\right|$ where $\mu = 2.5$ and 8.0, and clearly implies that the magnitude in the case of $\mu = 2.5$ is larger than that of $\mu = 8.0$. This result implies that the walking speed decreases when μ is small is not because it is impossible to drive the CoM in the direction of $\dot{\boldsymbol{r}}_g$ but because there exists a large unnecessary force in the direction perpendicular to $\dot{\boldsymbol{r}}_g$. Fig. 6 shows the conditions of $\boldsymbol{f}_g$ and its projection vectors for small and large μ. The magnitudes of ${}^{p}\boldsymbol{f}_g$ in both cases are almost equal to $Mg\tan\phi$, whereas those of ${}^{p}\boldsymbol{f}_g^{\perp}$ are different. In the case of small μ, it is clear that ${}^{p}\boldsymbol{f}_g^{\perp}$ increases the gravity and disturbs propelling the CoM forward to overcome the potential barrier at midstance.

IV. Biped Model with Semicircular Feet and Underactuated Virtual Passive Dynamic Walking

Now that we have discussed the mechanism of a flat feet model, in this section, let's investigate that of a semicircular feet model.

A. Model with semicircular feet

Let $\boldsymbol{\theta} = \begin{bmatrix}\theta_1 & \theta_2\end{bmatrix}^{\mathrm{T}}$ be the generalized coordinate vector and u_H be the hip-joint torque. The dynamic equation of the robot is then given by

$$\boldsymbol{M}(\boldsymbol{\theta})\ddot{\boldsymbol{\theta}} + \boldsymbol{C}(\boldsymbol{\theta},\dot{\boldsymbol{\theta}})\dot{\boldsymbol{\theta}} + \boldsymbol{g}(\boldsymbol{\theta}) = \boldsymbol{S}u_H = \begin{bmatrix}1\\-1\end{bmatrix}u_H. \tag{21}$$

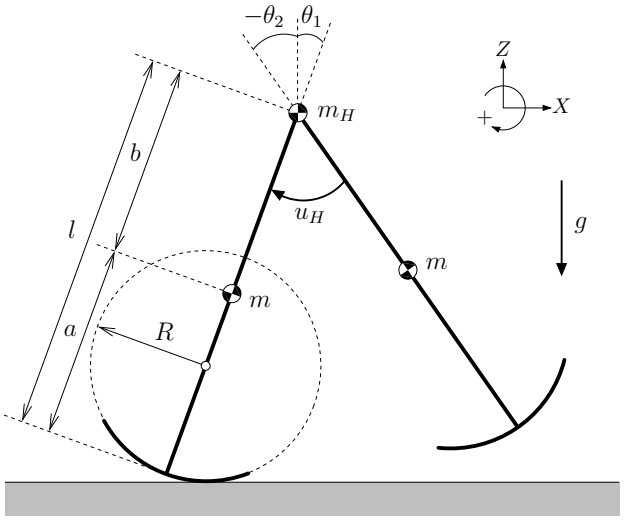

Fig. 7. Model of planar underactuated biped robot with semicircular feet

The details of the terms are as follows.

$$
\begin{aligned}
\boldsymbol{M}(\boldsymbol{\theta}) &= \begin{bmatrix} M_{11} & M_{12} \\ M_{21} & M_{22} \end{bmatrix},\ \boldsymbol{C}(\boldsymbol{\theta},\dot{\boldsymbol{\theta}}) = \begin{bmatrix} C_{11} & C_{12} \\ C_{21} & C_{22} \end{bmatrix} \\
M_{11} &= m\left(R^2 + (a-R)^2 + 2R(a-R)\cos\theta_1\right) \\
&\quad +(m_H+m)\left(R^2 + (l-R)^2 + 2R(l-R)\cos\theta_1\right) \\
M_{12} &= M_{21} = -mb\left(R\cos\theta_2 + (l-R)\cos\theta_H\right) \\
M_{22} &= mb^2 \\
C_{11} &= -mR(a-R)\dot{\theta}_1\sin\theta_1 \\
&\quad -(m_H+m)R(l-R)\dot{\theta}_1\sin\theta_1 \\
C_{12} &= mb\dot{\theta}_2(R\sin\theta_2 - (l-R)\sin\theta_H) \\
C_{21} &= mb(l-R)\dot{\theta}_1\sin\theta_H \\
C_{22} &= 0 \\
\boldsymbol{g}(\boldsymbol{\theta}) &= \begin{bmatrix} -\left(m_H l + ml + ma - MR\right)g\sin\theta_1 \\ mbg\sin\theta_2 \end{bmatrix}
\end{aligned}
$$

We denote the hip-joint torque and the relative hip-joint angle respectively as u_H and $\theta_H := \theta_1 - \theta_2$ in the meaning of distinguishing the underactuated model from the fully-actuated one.

B. Underactuated virtual passive dynamic walking

Time derivative of the mechanical energy in this case satisfies the relation $\dot{E} = \dot{\theta}_H u_H$. Virtual passive dynamic walking is then formulated as

$$\dot{E} = \dot{\theta}_H u_H = Mg\tan\phi\dot{X}_g, \tag{22}$$

and the hip-joint torque u_H is uniquely determined as

$$u_H = \frac{Mg\tan\phi\dot{X}_g}{\dot{\theta}_H}. \tag{23}$$

We call the walking style driven by only the hip-joint torque of Eq. (23) *underactuated virtual passive dynamic walking (UVPDW)* [5]. Eq. (23) has a singularity at $\dot{\theta}_H = 0$, but this does not make a matter because the system automatically avoid the singular point [5]. Limit cycle walkers often exhibit

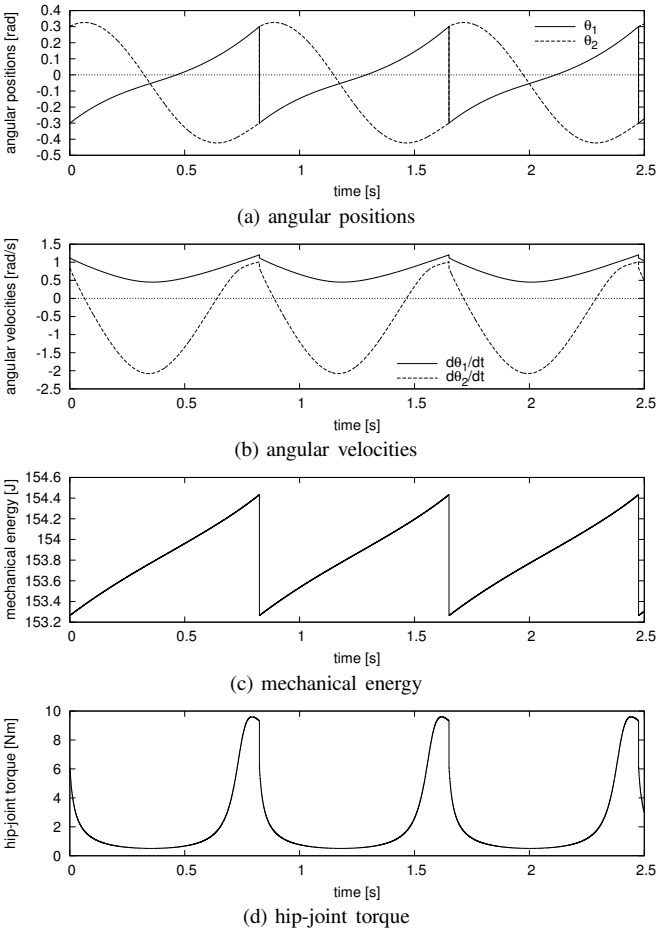

(a) angular positions
(b) angular velocities
(c) mechanical energy
(d) hip-joint torque

Fig. 8. Simulation results for underactuated virtual passive dynamic walking with semicircular feet where $\phi = 0.01$ [rad]

swing leg retraction [6] which is a motion of the swing leg; it moves backward just prior to the heel-strike. UVPDW systems, however, do not exhibit the motion regardless of the system parameter choice. The detailed mechanism should be described in another paper. Fig. 8 shows the simulation results for UVPDW where $R = 0.5$ [m] and $\phi = 0.01$ [rad]. Other system parameters are chosen as in Table I. We can see that from Fig. 8 (b), the condition $\dot{\theta}_1 > \dot{\theta}_2$ always holds, and from (d) the control input u_H does not diverge during a cycle. Fig. 9 shows the stick diagrams of UVPDW where (a) $\phi = 0.02$ and (b) $\phi = 0.03$ [rad]. In both cases, swing leg retraction does not occur; the singularity is automatically avoided.

If the condition $\dot{\theta}_H > 0$ holds, the maximum efficiency condition also holds. The energy-efficiency is evaluated by specific resistance defined as

$$\text{Specific resistance} = \frac{p}{Mgv}, \tag{24}$$

which means energy consumption per distance traveled per kilogram mass per gravity. p is the consumed input power, v is the walking speed, and are respectively defined as

$$p := \frac{1}{T}\int_{0^+}^{T^-} \left|\dot{\theta}_H u_H\right| \,\mathrm{d}t, \tag{25}$$

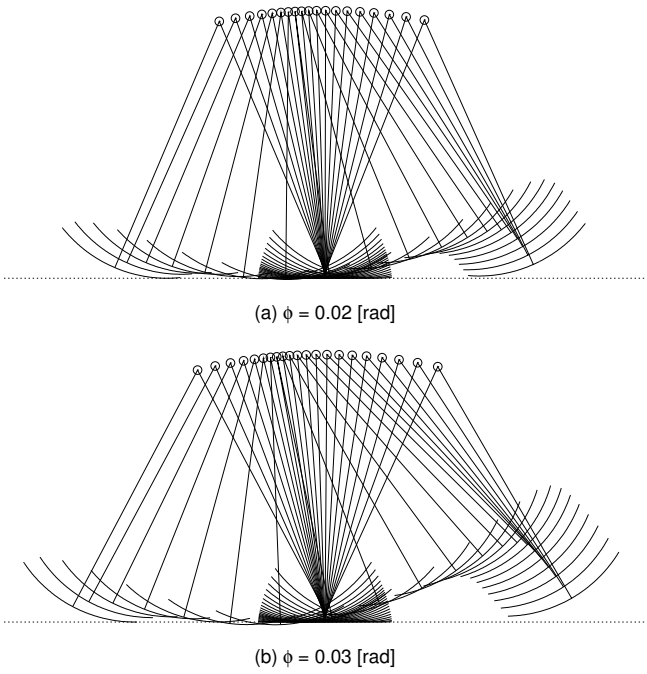

Fig. 9. Stick diagrams for underactuated virtual passive dynamic walking with semicircular feet

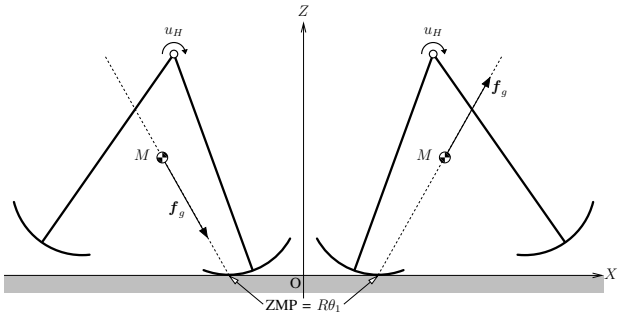

Fig. 10. Generalized virtual gravity in underactuated virtual passive dynamic walking with semicircular feet

$$v := \frac{1}{T}\int_{0^+}^{T^-} \dot{X}_g \, \mathrm{d}t = \frac{\Delta X_g}{T}. \tag{26}$$

Following these equations, the maximum efficiency condition is derived as

$$\frac{p}{Mgv} := \frac{\int_{0^+}^{T^-} \left|\dot{\theta}_H u_H\right| \, \mathrm{d}t}{Mg\Delta X_g} \geq \frac{\int_{0^+}^{T^-} \dot{\theta}_H u_H \, \mathrm{d}t}{Mg\Delta X_g} = \frac{\Delta E}{Mg\Delta X_g} \tag{27}$$

where $\Delta E := E(T^-) - E(0^+)$. Because of $\dot{\theta}_H > 0$ and $u_H > 0$, the equality in Eq. (27) holds and the maximum efficiency is achieved. Since $\Delta E = Mg\tan\phi\Delta X_g$ holds in the case of VPDW, the minimum specific resistance yields $\tan\phi$; UVPDW always achieves it.

C. On generalized virtual gravity

Let the contact point of the sole with the ground when $\theta_1 = 0$ be the central point of the X-Z coordinate, general X-position of the contact point yields $R\theta_1$. The point in this model is equivalent to the ZMP. The generalized virtual gravity vector of u_H yields

$$\boldsymbol{f}_g = \boldsymbol{J}_g(\boldsymbol{\theta})^{-\mathrm{T}} \begin{bmatrix} 1 \\ -1 \end{bmatrix} u_H = \frac{u_H}{\Delta_g}\left(\begin{bmatrix} R\theta_1 \\ 0 \end{bmatrix} - \boldsymbol{r}_g\right) \tag{28}$$

and is found to be the vector from the contact point to the CoM. As shown in Fig. 10, it acts as a centripetal force (left) or a centrifugal force (right).

Although there is an *unreasonableness* that the robot must be driven by only the central force during the cycle, the rolling effect overcomes it. In the next section, we deeply investigate the mechanism.

V. Investigating Rolling Effect through Comparison with Virtual Flat Feet Model

This section investigates the rolling effect through linearization and comparison of the semicircular feet model with the flat feet one.

A. Linearization and comparison of two models

Linearizing the semicircular feet model around the equilibrium point, $\boldsymbol{\theta} = \dot{\boldsymbol{\theta}} = \boldsymbol{0}_{2\times 1}$, the inertia matrix yields

$$\boldsymbol{M}_0 = \begin{bmatrix} m_H l^2 + ma^2 + ml^2 & -mbl \\ -mbl & mb^2 \end{bmatrix}, \tag{29}$$

and this does not have any terms concerning the foot radius, R. The linearization of the nonlinear vector, $\boldsymbol{C}\dot{\boldsymbol{\theta}}$, on the other hand, yields $\boldsymbol{0}_{2\times 1}$, and is equivalent to the flat feet model's result. The matrix $\boldsymbol{M}$ and the vector $\boldsymbol{C}\dot{\boldsymbol{\theta}}$ of the two models are equivalent in the sense of linearized system. The gravity term $\boldsymbol{g}(\boldsymbol{\theta})$ has a difference. That of the semicircular feet model can be divided into the following two terms.

$$\boldsymbol{g}(\boldsymbol{\theta}) = \begin{bmatrix} -(m_H l + ml + ma)\, g\sin\theta_1 \\ mbg\sin\theta_2 \end{bmatrix} + \begin{bmatrix} MRg\sin\theta_1 \\ 0 \end{bmatrix} \tag{30}$$

The first term of the right-hand side is the same as the gravity term of the flat feet model. The semicircular feet model is therefore equivalent to the flat feet one with the ankle-joint torque which is given as $-MRg\sin\theta_1$ in the meaning of linearized system. The virtual ankle-joint torque accelerates the CoM forward when $\theta_1 < 0$, whereas it decelerates in the case of $\theta_1 > 0$. The real hip-joint torque then accelerates the CoM forward effectively together with the virtual ankle-joint torque or the rolling effect. This driving mechanism is shown in Fig. 11; the CoM of the virtual flat feet model is suitably accelerated forward by the hip-joint torque reproducing the virtual gravity effect and the virtual ankle-joint torque.

This can be explained from angular momentum point of view. Time derivative of angular momentum, L, in the case with free ankle joint, should satisfy $\dot{L} = MgX_g$. The gravity effect then decreases the angular momentum when $X_g < 0$ and increases it when $X_g > 0$. The robot is accelerated automatically when $X_g > 0$ without any joint actuations and in this phase, after overcoming the potential barrier, the external driving force is not necessary. We thus need to exert some torques to drive the CoM forward during the first-half of cycle to overcome the potential barrier at midstance.

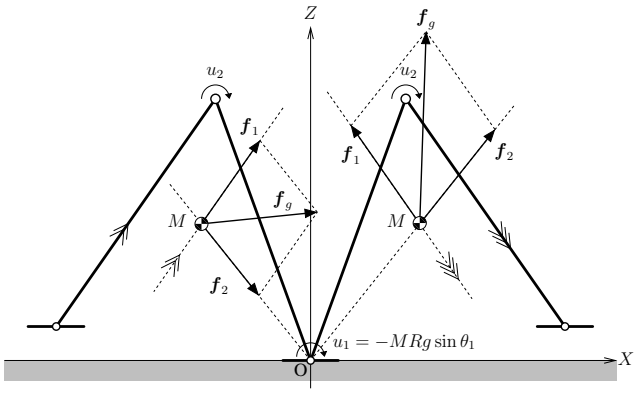

Fig. 11. Equivalent geometric relation of generalized virtual gravity vectors in Fig. 10

Note that the mechanical energy change done by the virtual ankle-joint torque is 0 because the following relation holds.

$$\int_{0^+}^{T^-} \dot{\theta}_1 \left(-MRg\sin\theta_1\right) \mathrm{d}t = MRg \int_{0^+}^{T^-} \frac{\mathrm{d}\cos\theta_1}{\mathrm{d}t}\mathrm{d}t$$
$$= MRg\left(\cos\left(\theta_1(T^-)\right) - \cos\left(\theta_1(0^+)\right)\right) = 0 \qquad (31)$$

Thus the mechanical energy restoration during the stance phase is executed by only the *real* hip-joint torque. Note that we use the relation $\theta_1(0^+) = -\theta_1(T^-)$ in the above calculation.

B. Typical gait of virtual flat feet model

In order to confirm the above results, we perform a numerical simulation of UVPDW using a virtual flat feet model with the virtual ankle-joint torque; a nonlinear fully-actuated flat feet model of Eq. (1) with the hip-joint torque of Eq. (23) and the virtual ankle-joint torque of $-MRg\sin\theta_1$. Note that we use the heel-strike's inelastic collision model not of the flat feet model but of the semicircular feet one because there is a serious difference for the mechanical energy dissipation. The semicircular feet decrease the energy dissipation but this paper does not discuss the detailed mechanism. We leave a detailed discussion about this for another opportunity. Fig. 12 shows the simulation results. The condition is the same as that of Fig. 8, and we can see that a similar gait is generated.

The total mechanical energy at $t = t_1$ ($0^+ \le t_1 \le T^-$) shown in Fig. 12 (c) is virtually calculated by

$$E(t_1) = E(0^+) + \int_{0^+}^{t_1} \dot{\theta}_H u_H \ \mathrm{d}t \qquad (32)$$

considering only the power input by the hip-joint torque. We can see that the mechanical energy exhibits the same orbit as the normal VPDW. Fig. 12 (e) shows the virtual ankle-joint torque and changes from positive to negative; this leads that the virtual ZMP travels in the virtual sole monotonically forward.

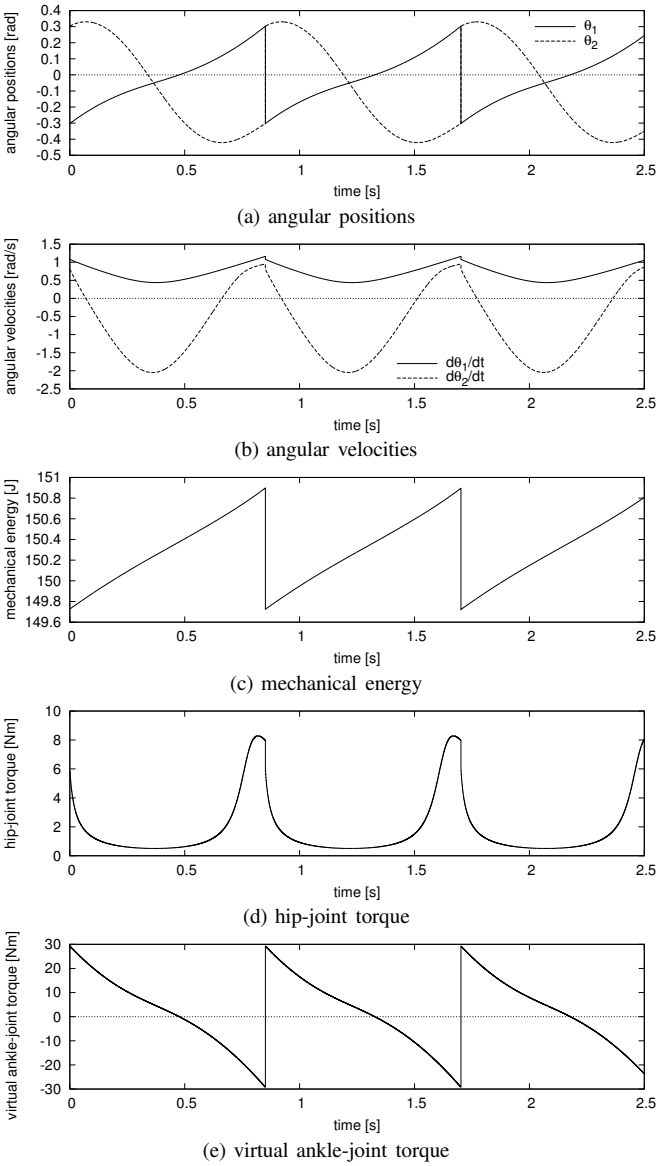

(a) angular positions
(b) angular velocities
(c) mechanical energy
(d) hip-joint torque
(e) virtual ankle-joint torque

Fig. 12. Simulation results for equivalent underactuated virtual passive dynamic walking of virtual flat feet model where $\phi = 0.01$ [rad]

C. Effect of foot radius on walking speed

The X-position at CoM is given by

$$X_g = R(\theta_1 - \sin\theta_1) + \frac{(m_H l + ma + ml)\sin\theta_1 - mb\sin\theta_2}{M}, \qquad (33)$$

and its time derivative yields

$$\dot{X}_g = R\dot{\theta}_1(1-\cos\theta_1) + \frac{(m_H l + ma + ml)\dot{\theta}_1\cos\theta_1 - mb\dot{\theta}_2\cos\theta_2}{M}. \qquad (34)$$

Note that $\cos\theta_1 \approx 1$ when θ_1 is sufficiently small and thus the first term of the right hand side of Eq. (34) is almost 0. We then find $\dot{X}_g$ is not affected by R directly. Although the foot radius R appears as the virtual ankle-joint torque to drive the CoM, it does not increase the CoM velocity

$\dot{X}_g$ directly. The authors consider that the reason why the semicircular feet increase the walking speed lies in the heel-strike mechanism.

VI. Conclusions

This paper investigated the mechanisms of planar compass-like biped robots with flat or semicircular feet based on the concept of generalized virtual gravity. The relation of a flat feet model between the CoM and the joint torques was firstly investigated and the importance of ankle-joint torque was theoretically clarified. It was numerically shown that UVPDW can be realized in the case with semicircular feet, and the relation between the rolling effect and the ankle-joint torque was clarified. In the second, a virtual flat feet model is introduced and the possibility is examined. The authors believe that walkers with semicircular feet should be treated not as a "synthetic wheel" McGeer considered but as a virtual fully-actuated system whose ankle-joint torque is determined uniquely by the foot radius R, the robot's total mass M and the stance-leg angle θ_1. This further implies that the optimal convex curve shape of feet can be designed if the optimal ankle-joint torque is determined. Further investigation is necessary.

VII. Acknowledgments

This work was partially supported by a Grant-in-Aid for Scientific Research, (B) No. 18360115, provided by the Japan Society for the Promotion of Science (JSPS).

References

[1] M. Vukobratović and J. Stepanenko, "On the stability of anthropomorphic systems," *Mathematical Biosciences*, vol.15, pp.1–37, 1972.

[2] T. McGeer, "Passive dynamic walking," *Int. J. of Robotics Research*, vol.9, no.2, pp.62–82, 1990.

[3] F. Asano and M. Yamakita, "Virtual gravity and coupling control for robotic gait synthesis," *IEEE Trans. on Systems, Man and Cybernetics Part A: Systems and Humans*, vol.31, no.6, pp.737–745, 2001.

[4] F. Asano, Z.W. Luo and M. Yamakita, "Biped gait generation and control based on a unified property of passive dynamic walking," *IEEE Trans. on Robotics*, vol.21, no.4, pp.754–762, 2005.

[5] F. Asano and Z.W. Luo, "On energy-efficient and high-speed dynamic biped locomotion with semicircular feet," *Proc. of the IEEE/RSJ Int. Conf. on Intelligent Robots and Systems (IROS)*, pp.5901–5906, 2006.

[6] A. Seyfarth, H. Geyer and H. Herr, "Swing-leg retraction: a simple control model for stable running," *J. of Experimental Biology*, vol.206, pp.2547–2555, 2003.

[7] A. Goswami, B. Espiau and A. Keramane, "Limit cycles in a passive compass gait biped and passivity-mimicking control laws," *Autonomous Robots*, vol.4, no.3, pp.273–286, 1997.

[8] R. Tedrake, T.W. Zhang, M. Fong and H.S. Seung, "Actuating a simple 3D passive dynamic walker," *Proc. of the IEEE Int. Conf. on Robotics and Automation (ICRA)*, pp.4656–4661, 2004.

[9] M. Wisse, A.L. Schwab, R.Q. van der Linde and F.C.T. van der Helm, "How to keep from falling forward: elementary swing leg action for passive dynamic walkers," *IEEE Trans. on Robotics*, vol.21, no.3, pp.393–401, 2005.